Efficient Mineralization of Organic Pollutants Using Visible-light-induced PTCDA Anions Electronic Reservoir and Photogenerated Holes

Yan Guo
Harbin Institute of Technology
Qixin Zhou
Tsinghua University
Jun Nan
Harbin Institute of Technology
Yongfa Zhu (zhuyf@tsinghua.edu.cn)
Tsinghua University https://orcid.org/0000-0001-8528-509X

Article

Keywords: Deep mineralization, PTCDA anion, Peroxymonosulfate, Photocatalysis

Posted Date: March 3rd, 2021

DOI: https://doi.org/10.21203/rs.3.rs-154817/v1

Abstract

Introducing the anion intermediate found with PTCDA into advanced oxidation processes (AOPs) overcomes the limitation of visible-light degradation. Stabilized PTCDA anionic intermediates act as electron reservoir to activate PMS to generate reactive oxygen species, thus improving the degradation rate of organic pollutants driven by visible light. At the same time, the photogenerated holes of PDI induce α and β scission with the unshared electron in organic molecules, and realize the deep mineralization of converting organic molecules to CO_2. The BPA degradation rate of PTCDA /PMS is over 125.8 and 2.8 times as high as PTCDA photocatalysis and Co_3O_4/PMS, respectively. The BPA mineralization of PTCDA /PMS reaching ~ 88% outclasses Co_3O_4/PMS (~ 25%). In continuous flow reactor, it has a ~ 100% degradation and ~ 80% mineralization of BPA. The outstanding degradation in real water under solar light excitation indicates that PTCDA/PMS would be an intriguing system for non-toxic and harmless elimination of organic pollutants.

Introduction

Advanced oxidation processes (AOPs) decompose complex organic pollutants into CO_2 and H_2O via reactive oxygen species (ROS) [1, 2, 3]. However, the toxicity of low-concentration intermediates produced without complete mineralization may threaten humans, ecosystems and the environment [4, 5, 6, 7, 8, 9]. Therefore, deep mineralization must be realized for water or water reuse. Nowadays, catalysts/cocatalysts that significantly promote the activation of oxidants (H_2O_2, peroxymonosulfate (PMS), etc.) have been widely investigated due to its fast rate of ROS production [10]. These ROS can decompose organic pollutants with high flux, but are difficult to completely oxidize to CO_2 [11]. Besides, PMS, for example, has a low utilization rate due to the limitations of poor invertibility of transition metals. The singlet oxygen ($^1O_2$) dominates the non-radical pathway [12, 13, 14, 15]. Especially for carbonaceous materials, $^1O_2$ produced by PMS self-decomposition is the main active species for degradation[16]. However, the oxidation potential of $^1O_2$ is not powerful enough to mineralize pollutants[17, 18, 19, 20, 21]. It is still a challenge to activate PMS by non-metallic catalysts with deep mineralization capabilities.

As another vital oxidation species, the photogenerated holes (h^+) produced in photocatalysis can react with organic compounds via dynamic control thus avoid the problem of sluggish kinetic to form CO_2. A deeper valence band (VB) often produce h^+ with stronger oxidation ability,[22] which can be controlled by adjusting the molecular structure of organic semiconductors.[23, 24] As for the degradation process caused by photogenerated holes in the photocatalytic process, there has always been vague questions: how does h^+ interact with organic pollutants? What is the mechanism responsible for mineralization? There is little in-depth literature on this issue. Therefore, it is of great significance to figure out how the h^+ plays a mineralize role in photocatalytic degradation process, which currently presents a key barrier to achieve deep mineralization of AOPs.

Recently, PTCDA-based supramolecular catalysts have been introduced in photocatalytic oxidation of water, producing oxygen by its h^+ with strong oxidation capacity generated by the low VB position[23, 25, 26]. It is reasonable to suspect that h^+ of PTCDA promotes the mineralization of organic pollutants. PTCDA anions generated by PTCDA under the light excitation have been used as an efficient electron donor in electron transfer system[27]. Fortunately, this hints that the production and elimination of anions in PTCDA is reversible. To be inspired, it is expected that the PTCDA anions generated by wide wavelength visible light will act as electrons reservoirs to activate PMS, triggering a chain reaction. Meanwhile, h^+ participates in degradation reaction to realize deep mineralization.

Herein, the PTCDA anion produced by photocatalysis was accurately used as an electron reservoir for activating PMS. The wide spectrum up to 700nm induced numerous PTCDA anions, providing an electronically activated PMS to realize a high-flux degradation process. Due to the strong adsorption of PMS and rapid reaction on PTCDA, the self-decomposition of PMS efficiency decreased to achieve high utilization of PMS. The timely removal of e^- promoted the effective participation of h^+ in the degradation process, leading to the occurrence of deep mineralization. The α and β scission of organic pollutants caused by photogenerated holes is the main mechanism of deep mineralization. As an AOP technology, its universal applicability to pollutants, super stability, excellent performance in the flow system, real water and solar light, indicating it is an extremely potential environmental remediation technology.

Results And Discussion

High-flux Degradation with Deep Mineralization for BPA by PTCDA/PMS system. With Bisphenol A (BPA) as a target pollutant, the catalytic degradation activity of PTCDA/PMS system was investigated. Compared with PTCDA photocatalysis, PTCDA/PMS has the advantage of high-flux degradation. The BPA removal in PTCDA photocatalysis was less than 10%. Interestingly, the coexistence of PMS and PTCDA boosted BPA removal efficiency significantly up to 100%. The highest degradation rate of PTCDA/PMS (0.629 min^{-1}) is 125.8 times that of PTCDA photocatalysis system (Fig. 1a). The PTCDA with different side chains such as alanine has the same phenomenon (Figure S1). A high concentration of 100 ppm BPA was entirely degraded by PTCDA/PMS system in 5 h, far better than the conventional Co_3O_4/PMS system (~ 50%) (Figure S2).The addition of PMS significantly increased the degradation abilities and 0.3 mM was chosen as the concentration for subsequent work considering the cost (Figure S3). Besides, the PTCDA/PMS system decomposed different organic pollutants rapidly, verifying that PTCDA/PMS was effective for the remediation of wastewater with various recalcitrant organic pollutants (Figure S4). After 5 cycles in batch reactor, ~ 100% of BPA was still removed within 10 min, and the morphology and structure after the reaction remained unchanged (Figure S5), indicating the excellent recirculation of PTCDA. Furthermore, a series of characterization showed that the superb charge transport ability of PTCDA laid a foundation for obtaining high-flux degradation performance (see Figure S24-S26 for detailed analysis).

Mineralization capacity is an important indicator to evaluate AOP. The removal of TOC reached ~ 88% for PTCDA/PMS system. However, the conventional single AOP is considered to be unable to completely oxidize and degrade organic pollutants.[28, 29, 30] For comparison, conventional Fenton-like

cocatalysts such as Co_3O_4, Fe_2O_3 and multi-walled carbon nanotubes (CNT) were selected to conduct BPA degradation and TOC removal tests (Fig. 1b), where PTCDA/PMS showed an absolute advantage. At a lower PMS dosage of 0.3 mM, Co_3O_4 and Fe_2O_3 could only completely degrade ~ 25% and ~ 13% of BPA into CO_2 respectively (Figure S7). The adsorption of CNT removed 39% of TOC, but only 5% comes from the activation of PMS (Figure S6). By further increasing the dosage of PMS to 1.0 mM, the mineralization for Co_3O_4, Fe_2O_3 and CNT obtained limited improvement (Figure S8), which was still far from that in PTCDA/PMS system. Homogeneous Fenton (Fe^{2+}/H_2O_2) is widely regarded as a powerful tool for removing organic pollutants, but its mineralization ability is poor. When 20ppm, 50ppm and 100ppm BPA as target pollutants, Fe^{2+}/H_2O_2 can only mineralize ~ 28%, ~ 30% and ~ 27% respectively. Surprisingly, the PTCDA/PMS system is ~ 88%, ~ 69% and ~ 55%, respectively (Figure S9). Admittedly, homogeneous Fenton can quickly remove the target pollutants, but it cannot completely oxidize and degrade them, making the target pollutants only stay in the intermediate stage. The PTCDA/PMS system obtained high-flux degradation with deep mineralization.

Since visible light accounts for ~ 45% of the total radiant energy of sunlight, a wide-spectrum response is particularly important[31]. Contributed by the π-π accumulation induced extended conjugated electron cloud, the edge of the intrinsic absorption band of PTCDA covers the entire visible range of 630nm, further calculating the bandgap of 1.97ev, the position of CB and VB is -0.33V and 1.64V, respectively (Figure S10). Expanding the absorption is beneficial to improve the ideal solar energy conversion efficiency since photon absorption is the first step of photocatalysis[32, 33]. In this regard, PTCDA with a large conjugate that can powerfully capture light is suitable. Moreover, the photogenerated charge on the PTCDA surface can be detected by the steady-state surface photovoltage (SPV) spectrum. The PTCDA produced an obviously positive signal in the 300–700 nm, with a maximum of 163 μV. The wavelength-dependent photocatalytic degradation activity of PTCDA/PMS system closely matches with SPV change trends (Fig. 1c). A positive signal indicates that photogenerated holes are transferred to the irradiated surface to oxidize BPA as the main reactive species.

How to improve the mineralization without significantly increasing the concentration of PMS is a crucial problem for the application of persulfate in the field of water and wastewater treatment[34, 35], which can be solved by PTCDA/PMS system. A low concentration of 0.3 mM PMS is added to PTCDA/PMS system, and 58.7mg BPA can be mineralized per millimole of PMS (Table S2). However, this value is 16.7, 8.7 and 3.3 for Co_3O_4, Fe_2O_3, and CNT respectively (Fig. 1d). So far, compared with PTCDA photocatalysis and conventional Fenton-like systems, PTCDA/PMS possesses high-flux deep mineralization and efficient use of PMS.

High-flux Degradation Mechanism. Because of the extensive system of conjugate π, PTCDA semiconductor is beneficial to store photogenerated electrons to form electron reservoir. First, a bias voltage was applied to prove that PTCDA could be converted to PTCDA anions to form electronic reservoirs. The PTCDA showed an onset reduction potential of -1.015 V versus ferrocene (Figure S11), which corresponded to the formation of its anion ($PTCDA^-$), while the second onset reduction potential at -1.269 V indicated the transformation from $PTCDA^-$ to the dianion state ($PTCDA^{2-}$). Whether it was $PTCDA^-$ or $PTCDA^{2-}$, such a low potential can reduce PMS. Meanwhile, light excitation could produce PTCDA anion as well[36, 37].

The PTCDA anions exhibited a different color from their own that enabled them to be tested by ultraviolet-visible (UV-Vis) light irradiation [38, 39]. New absorption bands of PTCDA anion appeared at ~ 668, ~755 and ~ 788 nm under irradiation of λ≥350 nm, and the maximum amount of PTCDA anions was obtained when irradiated with simulated sunlight (Fig. 2a). With the prolongation of the irradiation time, the absorption of PTCDA anions increased sharply (Figure S12a). However, UV-vis absorption of PTCDA anion in PMS solution was relatively weak even for more extended periods of light irradiation (Figure S12b). To give more evidence, the PTCDA anion could be observed by electron paramagnetic resonance (EPR) since the unpaired electrons on the PTCDA anion. As shown in the illustration in Fig. 2b, a strong resonance with a g = 2.00359 was detected after illumination, and no hyperfine splitting information indicated complete delocalization of unpaired electrons on PTCDA[40, 41]. In order to quantify the content of PTCDA anions, the EPR signal peak and the standard manganese peak were integrated separately, and the ratio of the two was taken[42, 43]. After turning off the light, the signal was significantly weakened and stabilized (Figure S13a). With the extension of irradiation, the PTCDA anion signal gradually increased. Turning off the light for 17 min, the PTCDA free radical signal was still stronger than initial dark state (Figure S13b), indicating that PTCDA anion forms a stable electronic reservoir. Surprisingly, PTCDA anions tested in water could almost be reduced to a dark state (Figure S13c-d) due to electrons were captured by abundant electron acceptors (H_2O, O_2). In the presence of electron acceptors, the electron reservior provided electrons, making the generation and quenching of PTCDA anion a reversible process. As expected, the PTCDA anion in PMS solution is weak (Figure S14). Similar to H_2O or O_2, the PMS as an electron acceptor takes electrons from the PTCDA anion electron reservior. Besides, Alanine-PTCDA has the same phenomenon (Figure S15-16). The above results strongly proved that PTCDA anion served as an electron reservoir for PMS under wide spectrum excitation, resulting in the activation of PMS and occurrence of Fenton-like reaction. Besides, the order of the degradation rate in different atmospheres was as follow: $k_2(N_2) > k_2(Air) > k_2(O_2)$, which emphasized the importance of PMS activation by PTCDA anion electron reservoir (Figure S17). The intense adsorption energy between PMS and PTCDA (-87.35kJ/mol) suggested that PTCDA could inhibit the self-decomposition of PMS (Figure S18), which was beneficial to improving the utilization rate of PMS.

Deep mineralization Mechanism. The quench experiment was used to explore the active species in PTCDA/PMS system. The degradation experiments were carried out by NaN_3 quenching $^1O_2$, P-BQ quenching $\cdot O_2^-$, TBA quenching ·OH, MeOH quenching ·OH, $\cdot SO_4^{2-}$, and HCOOH quenching h^+. After quenching h^+, the apparent rate constant decreased significantly (Fig. 3a), indicating that h^+ was the main active substance. The h^+ played such an important role based on the successful separation of e–h^+ by PMS. It can be proved through the composite constant of the average photogenerated charge expressed by open-circuit voltage (OCV) signal and the first-order dynamic model[44, 45]. The OCV attenuation rate of the PTCDA working electrode was $K = 7\times10^{-5}$ s^{-1} in PMS solution after turning off, which was 74% slower than that of $K = 27\times10^{-5}$ s^{-1} without PMS. (Fig. 3b. See support information for detailed analysis). The reason is that e^- of PTCDA anion was captured by PMS, resulting in the less e–h^+ recombination on PTCDA electrode surface, thus obtaining a long life of h^+.

As mentioned above, the mineralization of PTCDA/PMS with h^+ is much better than that of other Fenton-like systems, which is explained from the perspective of degradation products next. For the conventional Fenton-like system without h^+, a high concentration of hydroxyl admixture was captured by high resolution

mass spectrometry (LC/MS). Due to the hydroxyl radicals increased into the π electrons of BPA, hardly opened benzene ring for further mineralization[46]. The possible addition sites of BPA were predicted by Fukui function, which was consistent with the hydroxyl addition products detected by high- resolution LC/MS (Figure S19). On the contrary, small molecular weight substances were detected during the PTCDA/PMS (Fig. 3c), based on which possible degradation pathways can be inferred. h^+ produced in photocatalysis can react with organic compounds with thermodynamic control thus avoid the problem of sluggish kinetic. Based on several high-concentration intermediate products detected, a possible degradation process dominated by h^+ is speculated. h^+ firstly reacts with BPA through charge transfer and produces BPA free radical ($C_{15}H_{16}O_2^{\cdot-}$). Subsequently, $C_9H_{11}O^+$ and $C_6H_5O^\bullet$ are produced by β scission. $C_6H_5O^\cdot$ is activated to produce small molecular organic compounds which have been widely reported[47, 48]. $C_9H_{11}O^+$ produces $C_9H_{10}O$ (M = 134.0732) or/and $C_9H_{12}O_2$ (M = 152.0837) through hydrogen transfer and other reactions. $C_9H_{10}O$ (M = 134.0732) further forms $C_8H_8O_2$ (M = 136.0524) through h^+ reaction and α scission. The α-positions of the phenolic hydroxyl groups of $C_8H_8O_2$ (M = 136.0524) and $C_9H_{12}O_2$ (M = 152.0837) are active, and γH rearrangement can occur after reaction with h^+, which in turn causes α scission, leading to the benzene ring to open. Using DMPO as the trapping agent, EPR detected the six peaks with A_N= 14.7 Gauss hyperfine division constant (one of which was covered by the PTCDA anion peak), which belongs to the alkane free radical ($R^\bullet$) signal. The six-fold peak did not appear without BPA (Figure S20). Although it is impossible to determine the organic molecules of $R^\cdot$, but sufficient to account for the generation of $R^\cdot$ in PTCDA/PMS system. The EPR of $R^\cdot$ once again proving the rationality of the above speculation process. h^+ is positively charged, and their activation sites are atoms with unshared electrons, causing α and β scission, which is a process of rapid carbon reduction mineralization. All organic molecules with hydroxyl functional groups can be converted into small molecules by photogenerated holes in a similar way until mineralization.

So far, as Scheme 1 shows, PTCDA supramolecular generates PTCDA anion electron reservoir under wide spectral excitation. PMS obtains electrons from the electron reservoir to produce ROS (Figure S21), which can form rapidly hydroxyl admixture with BPA and/or incompletely degradation. h^+ rapidly mineralize organic molecules containing lone electrons through α and β scission.

Continuous Flow,real water and solar light Purification. Besides batch reactor, continuous flow performance is a key indicator to verify that purification technology is potential for industrial application. The purification effect of PTCDA/PMS was tested in a continuous flow reactor (Fig. 4a), which was illuminated by a 7.0 cm×2.5 cm×1.0 cm quartz window with a light area of 17.5 cm^2 (Fig. 4b). Non-woven fabrics fixed PTCDA powder is easy for recovery. With a treatment capacity of 34.3 L h^{-1} m^{-2}, the 10 mg/L BPA was completely purified in 50 h (Fig. 4c left). The mineralization maintained at ~ 80%. In contrast, for PTCDA photocatalysis, the removal of BPA is only ~ 2%. For Co_3O_4, the removal BPA reached ~ 74% within 1 hour. However, the removal rate was only ~ 25% and the mineralization was stable at ~ 5% after 9 h. Besides, in tap water, Songhua river and secondary sedimentation tank effluent tests with 20 mg/L BPA added, PTCDA/PMS system still obtained considerable degradation activity (Fig. 4c middle & Table S3). Although the xenon lamp used in the above experiment can simulate sunlight (Figure S22), to further demonstrate the industrial application potential of PTCDA/PMS system, degradation performance was tested under solar light. The sunlight intensity on the ground at 116.33° east longitude and 40.0° north latitude in autumn is ~ 60 mW/cm^2. PTCDA/PMS can degrade 10 mg/L BPA rapidly in 10 minutes under outdoor natural light exposure (Fig. 4c right & Figure S23). Based on high-flux deep mineralization, high stability and cost considerations, we believe that the PTCDA/PMS configuration should be an ideal oxidation system for the removal and mineralization of organic pollutants with high potential.

Conclusion

In summary, PTCDA/PMS system, a new AOP technology that achieved both high-flux degradation and deep mineralization of organic pollutants has been established. The high utilization rate of PMS conduces to high-flux degradation rate and occurs efficient photogenerated e^--h^+ separation. h + with high oxidizing ability produced α and β scission contributing to deep mineralization process far superior conventional Fenton-like process. This work provides a new solution for water environmental remediation.

Materials And Methods.

Synthesis perylenetetracarboxylic dianhydride and their derivatives (PTCDA). In this work, we have synthesized two types of perylene-based organic catalysts:

PTCDA 

Alanine-PTCDA 

Preparation of perylenetetracarboxylic dianhydride (PTCDA): Herein, we selected concentrated sulfuric acid and water to form mixed solvent systems of H_2SO_4/H_2O. Typically, 0.1g commercial PTCDA (perylenetetracarboxylic dianhydride, Alfa Aesar) was dissolved in 10mL H_2SO_4 (good solvent) under ultrasonic treatment for 1 hour, and then deionized water (poor solvent) of 100 mL were added into the above solution all at once, respectively. Solid insoluble precipitates would appear instantly and keep these suspensions still for another 0.5 h, and these resulting bright red solids were collected by filtration through a 0.45μm membrane filter and washed with deionized water for several times, and then dried in oven at 60°C for subsequent use. It is marked as PTCDA.

Preparation Alanine substituted PTCDA (Alanine-PTCDA): Perylene-3,4,9,10-tetracarboxylic dianhydride, 18 g imidazole and 2.5 g (28.06 mM) 3-aminopropionic acid (all supplied by Aldrich) were heated in a flask at 150°C for 4 h. Next, the reaction mixture was dispersed in 300 mL HCl (2 M) and 100 mL ethanol and stirred overnight. Then, the final red solid was washed to neutrality with distilled water and filtered through a 0.22 μm membrane filter. Finally,

the collected red solid was dried in an oven at 60°C under vacuum. Disperse 0.276 g of the above powder in 100 mL of water. Then add 417 μl of triethylamine solution and stir vigorously for about 30 minutes. Then add 20ml HCl (4M) and stir for another 3h. Centrifuge and wash the product to neutrality. Finally, the solid was collected and dried under vacuum at 60°C and made into powder. Labeled as alanine-PTCDA.

Non-woven fabric load of PTCDA photocatalysts. First, some clean hydrophilic non-woven fabrics are used as carriers for powdered PTCDA, and 20 mg of powdered PTCDA is dispersed in water and drip-coated on the non-woven fabric. The 5 oxygen atoms exposed by PTCDA can easily form hydrogen bonds with the hydrophilic non-woven fabric, which ensures that the PTCDA is firmly bonded to the non-woven fabric and avoids the leakage of the catalyst. Therefore, the successful loading of PTCDA on non-woven fabrics is a green and energy-saving way that does not require special catalyst recovery.

Non-woven fabric load of Co_3O_4 photocatalysts. The catalyst on non-woven fabric was replaced with Co_3O_4.

Declarations

Funding.

This work was supported by National Science Foundation of China (21872077), National Key Research and Development Project of China (2020YFA0710304),

Author Contributions.

J.N. and Y.Z. conceived this project. Q.Z designed the experiments. Y.G. conducted all experiments, characterizations and performed the analysis with constructive discussions. All authors contributed in discussing the results and writing the manuscript.

Conflict of interest statement. None declared.

References

1. Liu YQ, He XX, Duan XD, Fu YS, Fatta-Kassinos D, Dionysiou DD. Significant role of UV and carbonate radical on the degradation of oxytetracycline in UV-AOPs: Kinetics and mechanism. *Water Res* **95**, 195–204 (2016).
2. Li H, Shang J, Yang Z, Shen W, Ai Z, Zhang L. Oxygen Vacancy Associated Surface Fenton Chemistry: Surface Structure Dependent Hydroxyl Radicals Generation and Substrate Dependent Reactivity. *Environ Sci Technol* **51**, 5685–5694 (2017).
3. Zhu L, *et al.* Designing 3D-MoS2 Sponge as Excellent Cocatalysts in Advanced Oxidation Processes for Pollutant Control. *Angewandte Chemie-International Edition* **59**, 13968–13976 (2020).
4. Wang W-L, Wu Q-Y, Du Y, Huang N, Hu H-Y. Elimination of chlorine-refractory carbamazepine by breakpoint chlorination: Reactive species and oxidation byproducts. *Water Res* **129**, 115–122 (2018).
5. Escher BI, Fenner K. Recent Advances in Environmental Risk Assessment of Transformation Products. *Environ Sci Technol* **45**, 3835–3847 (2011).
6. Prasse C, Stalter D, Schulte-Oehlmann U, Oehlmann J, Ternes TA. Spoilt for choice: A critical review on the chemical and biological assessment of current wastewater treatment technologies. *Water Res* **87**, 237–270 (2015).
7. Haddad T, Baginska E, Kümmerer K. Transformation products of antibiotic and cytostatic drugs in the aquatic cycle that result from effluent treatment and abiotic/biotic reactions in the environment: An increasing challenge calling for higher emphasis on measures at the beginning of the pipe. *Water Res* **72**, 75–126 (2015).
8. Wang W-L, Wu Q-Y, Huang N, Xu Z-B, Lee M-Y, Hu H-Y. Potential risks from UV/H2O2 oxidation and UV photocatalysis: A review of toxic, assimilable, and sensory-unpleasant transformation products. *Water Res* **141**, 109–125 (2018).
9. Le Pivert M, Poupart R, Capochichi-Gnambodoe M, Martin N, Leprince-Wang Y. Direct growth of ZnO nanowires on civil engineering materials: smart materials for supported photodegradation. *Microsystems & Nanoengineering* **5**, 57 (2019).
10. Li L, *et al.* Degradation of naphthalene with magnetic bio-char activate hydrogen peroxide: Synergism of bio-char and Fe-Mn binary oxides. *Water Res* **160**, 238–248 (2019).
11. Ma J, *et al.* Fenton Degradation of Organic Pollutants in the Presence of Low-Molecular-Weight Organic Acids: Cooperative Effect of Quinone and Visible Light. *Environ Sci Technol* **40**, 618–624 (2006).
12. Chen C, *et al.* In-situ pyrolysis of Enteromorpha as carbocatalyst for catalytic removal of organic contaminants: Considering the intrinsic N/Fe in Enteromorpha and non-radical reaction. *Appl Catal B* **250**, 382–395 (2019).
13. Zhang W, *et al.* Synergy of nitrogen doping and structural defects on hierarchically porous carbons toward catalytic oxidation via a non-radical pathway. *Carbon N Y* **155**, 268–278 (2019).
14. Ye S, *et al.* Nitrogen-doped biochar fiber with graphitization from Boehmeria nivea for promoted peroxymonosulfate activation and non-radical degradation pathways with enhancing electron transfer. *Appl Catal B* **269**, (2020).
15. Wang N, Ma W, Ren Z, Du Y, Xu P, Han X. Prussian blue analogues derived porous nitrogen-doped carbon microspheres as high-performance metal-free peroxymonosulfate activators for non-radical-dominated degradation of organic pollutants. *J Mater Chem A* **6**, 884–895 (2018).
16. Lee J, von Gunten U, Kim J-H. Persulfate-Based Advanced Oxidation: Critical Assessment of Opportunities and Roadblocks. *Environ Sci Technol* **54**, 3064–3081 (2020).
17. Matsuura T. Bio-mimetic oxygenation. *Tetrahedron* **33**, 2869–2905 (1977).
18. Kearns DR. Physical and chemical properties of singlet molecular oxygen. *Chem Rev* **71**, 395–427 (1971).

19. Scully FE, Hoigné J. Rate constants for reactions of singlet oxygen with phenols and other compounds in water. *Chemosphere* **16**, 681–694 (1987).
20. Frimer AA. The reaction of singlet oxygen with olefins: the question of mechanism. *Chem Rev* **79**, 359–387 (1979).
21. Cheng X, Guo H, Zhang Y, Wu X, Liu Y. Non-photochemical production of singlet oxygen via activation of persulfate by carbon nanotubes. *Water Res* **113**, 80–88 (2017).
22. Zhang Z, *et al.* Photogenerated-hole-induced rapid elimination of solid tumors by the supramolecular porphyrin photocatalyst. *National Science Review*, (2020).
23. Guo Y, Li H, Ma W, Shi W, Zhu Y, Choi W. Photocatalytic activity enhanced via surface hybridization. *Carbon Energy* **2**, 308–349 (2020).
24. He ZC, *et al.* Simultaneous Enhancement of Open-Circuit Voltage, Short-Circuit Current Density, and Fill Factor in Polymer Solar Cells. *Adv Mater* **23**, 4636-+ (2011).
25. Zhang Z, Chen X, Zhang H, Liu W, Zhu W, Zhu Y. A Highly Crystalline Perylene Imide Polymer with the Robust Built-In Electric Field for Efficient Photocatalytic Water Oxidation. *Adv Mater* **32**, 1907746 (2020).
26. Yuan Y-J, *et al.* Metal-free broad-spectrum PTCDA/g-C_3N_4 Z-scheme photocatalysts for enhanced photocatalytic water oxidation. *Appl Catal B* **260**, 118179 (2020).
27. Ghosh I, Ghosh T, Bardagi JI, Konig B. Reduction of aryl halides by consecutive visible light-induced electron transfer processes. *Science* **346**, 725–728 (2014).
28. Augugliaro V, Litter M, Palmisano L, Soria J. The combination of heterogeneous photocatalysis with chemical and physical operations: A tool for improving the photoprocess performance. *Journal of Photochemistry and Photobiology C: Photochemistry Reviews* **7**, 127–144 (2006).
29. Demir F, Atguden A. Experimental Investigation on the Microbial Inactivation of Domestic Well Drinking Water using Ozone under Different Treatment Conditions. *Ozone-Sci Eng* **38**, 25–35 (2016).
30. Peller J, Wiest O, Kamat PV. Synergy of Combining Sonolysis and Photocatalysis in the Degradation and Mineralization of Chlorinated Aromatic Compounds. *Environ Sci Technol* **37**, 1926–1932 (2003).
31. Chen X, Xu Y, Ma X, Zhu Y. Large dipole moment induced efficient bismuth chromate photocatalysts for wide-spectrum driven water oxidation and complete mineralization of pollutants. *National Science Review* **7**, 652–659 (2020).
32. Wang Q, Domen K. Particulate Photocatalysts for Light-Driven Water Splitting: Mechanisms, Challenges, and Design Strategies. *Chem Rev* **120**, 919–985 (2020).
33. Zhang Z, Chen X, Zhang H, Liu W, Zhu W, Zhu Y. A Highly Crystalline Perylene Imide Polymer with the Robust Built-In Electric Field for Efficient Photocatalytic Water Oxidation. *Adv Mater* **32**, (2020).
34. Wang S, Wang J. A novel strategy of successive non-radical and radical process for enhancing the utilization efficiency of persulfate. *Chemosphere* **245**, 125555 (2020).
35. Wang Z, Bush RT, Sullivan LA, Chen C, Liu J. Selective Oxidation of Arsenite by Peroxymonosulfate with High Utilization Efficiency of Oxidant. *Environ Sci Technol* **48**, 3978–3985 (2014).
36. Lu C, Fujitsuka M, Sugimoto A, Majima T. Unprecedented Intramolecular Electron Transfer from Excited Perylenediimide Radical Anion. *The Journal of Physical Chemistry C* **120**, 12734–12741 (2016).
37. Zeman CJ, Kim S, Zhang F, Schanze KS. Direct Observation of the Reduction of Aryl Halides by a Photoexcited Perylene Diimide Radical Anion. *J Am Chem Soc* **142**, 2204–2207 (2020).
38. Xu Y, *et al.* Consecutive Charging of a Perylene Bisimide Dye by Multistep Low-Energy Solar-Light-Induced Electron Transfer Towards H2 Evolution. *Angew Chem Int Ed Engl* **59**, 10363–10367 (2020).
39. Zeng L, Liu T, He C, Shi D, Zhang F, Duan C. Organized Aggregation Makes Insoluble Perylene Diimide Efficient for the Reduction of Aryl Halides via Consecutive Visible Light-Induced Electron-Transfer Processes. *J Am Chem Soc* **138**, 3958–3961 (2016).
40. Schmidt D, Bialas D, Würthner F. Ambient Stable Zwitterionic Perylene Bisimide-Centered Radical. *Angewandte Chemie International Edition* **54**, 3611–3614 (2015).
41. Zhang A, Jiang W, Wang Z. Fulvalene-Embedded Perylene Diimide and Its Stable Radical Anion. *Angewandte Chemie International Edition* **59**, 752–757 (2020).
42. Wu C, *et al.* Mesoporous Polymeric Cyanamide-Triazole-Heptazine Photocatalysts for Highly-Efficient Water Splitting. *Small* **16**, 2003162 (2020).
43. Eaton GR, Eaton SS, Barr DP, Weber RT. *Quantitative EPR* (2010).
44. Jiang ZF, *et al.* Nature-based catalyst for visible-light-driven photocatalytic CO2 reduction. *Energy Environ Sci* **11**, 2382–2389 (2018).
45. Kim J, Monllor-Satoca D, Choi W. Simultaneous production of hydrogen with the degradation of organic pollutants using TiO2 photocatalyst modified with dual surface components. *Energy Environ Sci* **5**, 7647–7656 (2012).
46. Xiao R, *et al.* Mechanistic insight into degradation of endocrine disrupting chemical by hydroxyl radical: An experimental and theoretical approach. *Environ Pollut* **231**, 1446–1452 (2017).
47. Zazo JA, Casas JA, Mohedano AF, Gilarranz MA, Rodriguez JJ. Chemical pathway and kinetics of phenol oxidation by Fenton's reagent. *Environ Sci Technol* **39**, 9295–9302 (2005).
48. Sun B, Vorontsov AV, Smirniotis PG. Role of platinum deposited on TiO2 in phenol photocatalytic oxidation. *Langmuir* **19**, 3151–3156 (2003).

Figures

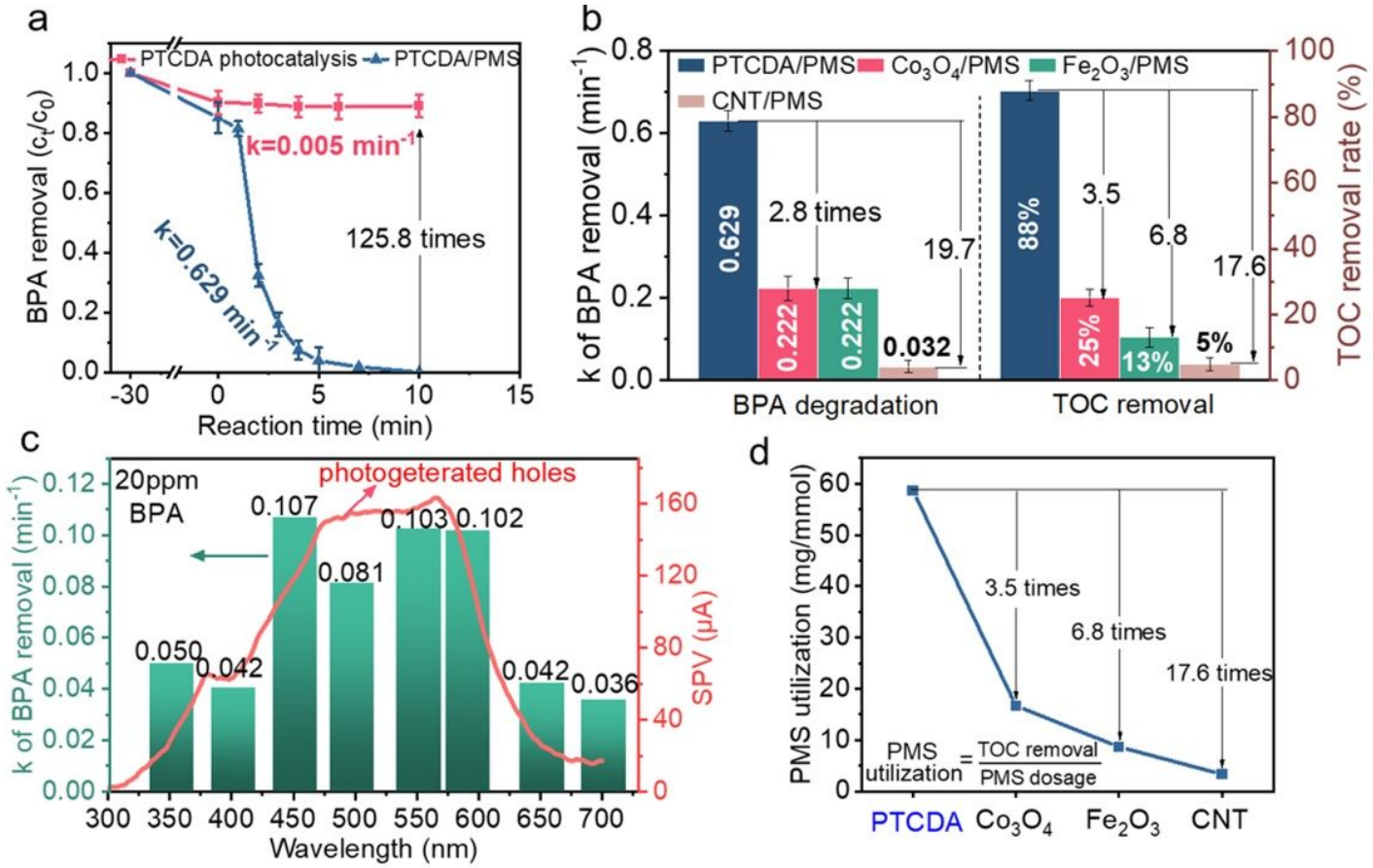

Figure 1

(a) Degradation of BPA by PTCDA photocatalysis with and without PMS. (b)BPA degradation and mineralization in different catalyst/PMS systems. The light is λ ≥ 420 nm and the intensity are ~300 mW/cm2. (c) Overlayer of wavelength-dependent BPA degradation rate constants k of PTCDA/PMS system and surface photovoltage (SPV) spectrum. (d) Comparison of the utilization of PMS in different catalysts /PMS systems. [catalyst] = 0.4 g L-1, [BPA] = 0.02 g L−1, [PMS] = 0.09 g L−1 and temperature = 20°C. The light intensity at different wavelengths is shown in the support information.

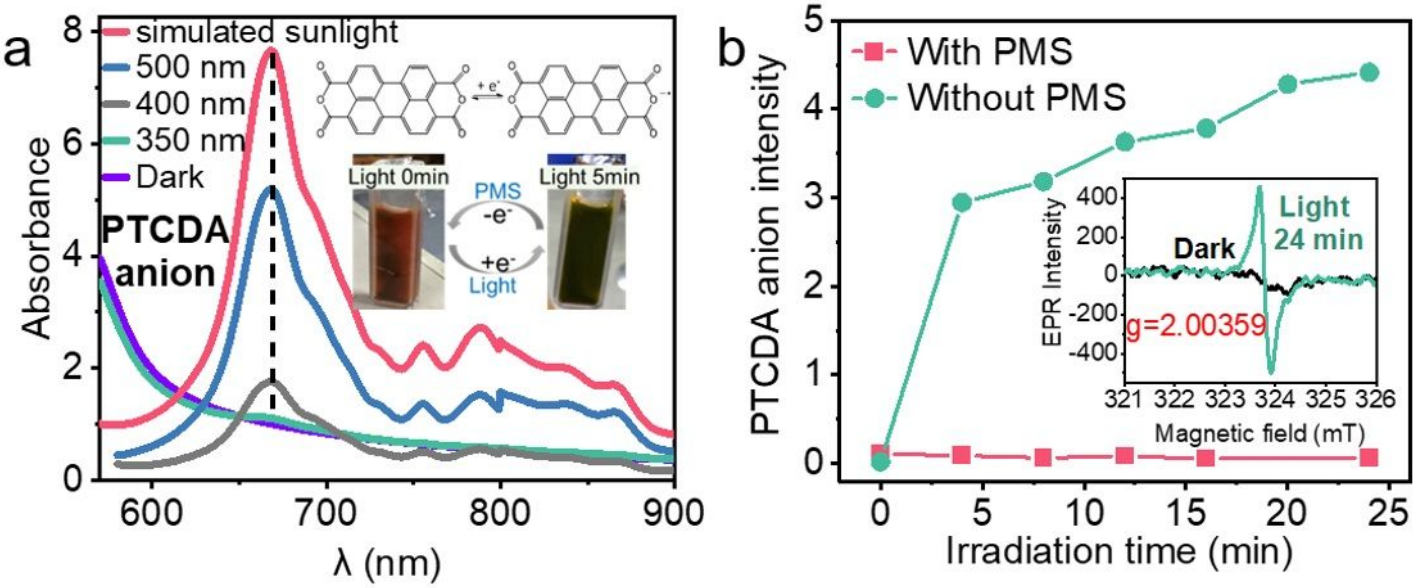

Figure 2

(a) UV-Vis absorption spectra of PTCDA (0.025 g L−1) in dimethylformamide (DMF) in the presence of DMPO (0.2 M) in the dark and expose to different wavelengths of light for 3 min. (b) Semi-quantitative PTCDA anion came from the EPR signal of PTCDA dispersed in water or 0.3 mM PMS solution. Inset in (b) shows the EPR signal in water.

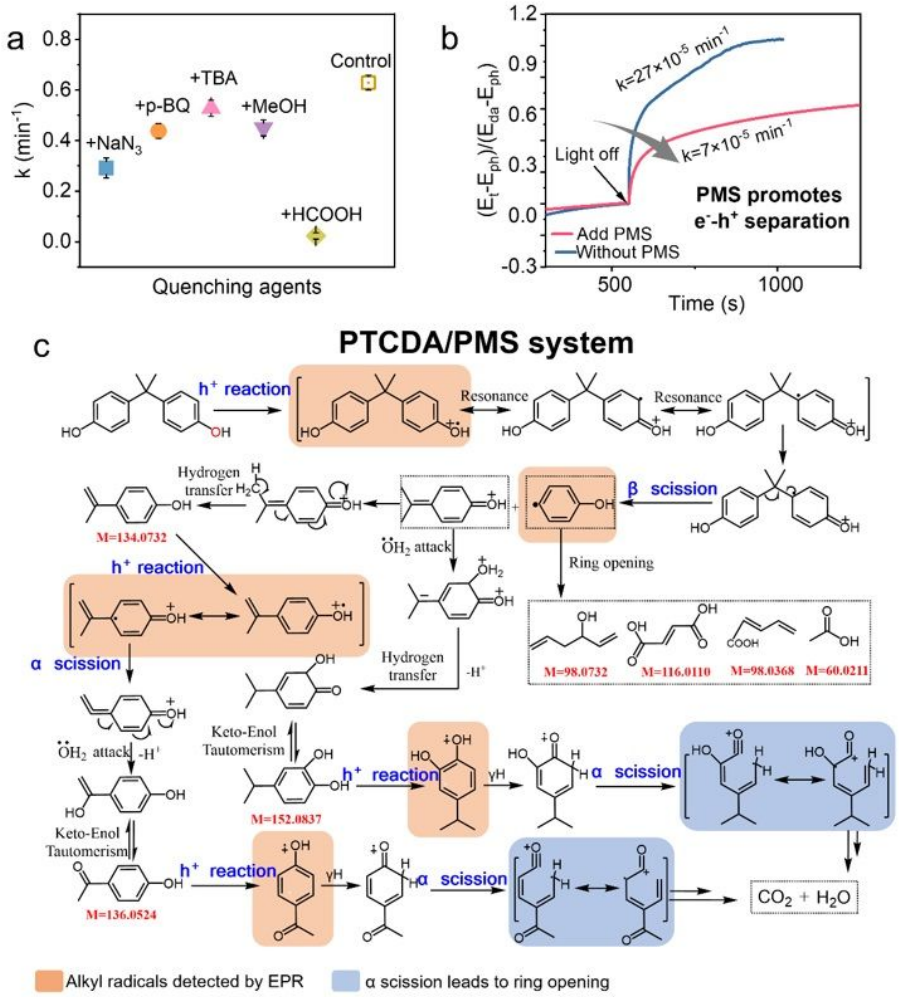

Figure 3

(a) The quenching experiment of different quenchers on the degradation of BPA in PTCDA/PMS photocatalytic system. (b) Normalized open-circuit potential (OCP) attenuation curves after turning off the λ≥420 nm irradiation for different systems. (c) The speculated path of the hole reaction with BPA in PTCDA/PMS system with photogenerated holes introduced.

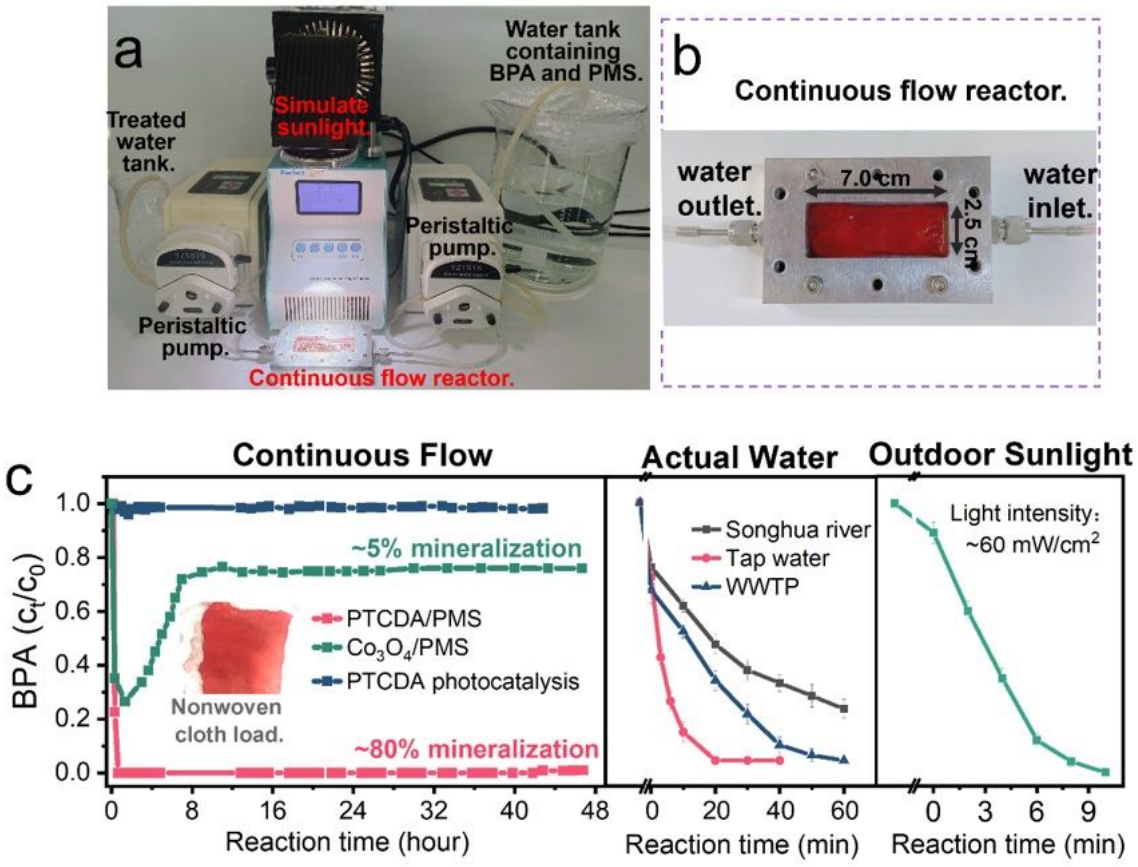

Figure 4

(a) Photograph of the continuous flow degradation device. (b) A detailed view of the continuous flow reactor. (c) Left: the removal effect of BPA in continuous flow reactor in different systems. The light is λ ≥ 420 nm and the intensity are ~300 mW/cm2.Middle: The BPA degradation effect of PTCDA/PMS system in actual water. The light is λ ≥ 420 nm and the intensity are ~300 mW/cm2. Right: Outdoor sunlight excitation testing of BPA degradation effect of PTCDA/PMS system in autumn in Beijing. Working conditions: [catalyst] = 20 mg, [BPA] = 0.01 g L−1, [PMS] = 0.09 g L−1 and temperature = 20 °C.

Supplementary Files

This is a list of supplementary files associated with this preprint. Click to download.

- SupportingInformation.docx